



UNIVERSITÀ DI PARMA

ARCHIVIO DELLA RICERCA

University of Parma Research Repository

Mechanical characterization of autoclaved aerated concrete masonry subjected to in-plane loading:
Experimental investigation and FE modeling

This is the peer reviewed version of the following article:

Original

Mechanical characterization of autoclaved aerated concrete masonry subjected to in-plane loading:
Experimental investigation and FE modeling / Ferretti, Daniele; Michelini, Elena; Rosati, Gianpaolo. - In:
CONSTRUCTION AND BUILDING MATERIALS. - ISSN 0950-0618. - 98:(2015), pp. 353-365.
[10.1016/j.conbuildmat.2015.08.121]

Availability:

This version is available at: 11381/2801037 since: 2021-10-21T15:31:21Z

Publisher:

Elsevier Ltd

Published

DOI:10.1016/j.conbuildmat.2015.08.121

Terms of use:

Anyone can freely access the full text of works made available as "Open Access". Works made available

Publisher copyright

note finali coverpage

(Article begins on next page)

Mechanical characterization of autoclaved aerated concrete masonry subjected to in-plane loading: experimental investigation and FE modeling

Daniele Ferretti^a *, Elena Michellini^a and Gianpaolo Rosati^b

^a *Department of Civil, Environmental, Land Management Engineering and Architecture,
University of Parma, P.co Area delle Scienze 181/A, 43124 Parma, Italy,
daniele.ferretti@unipr.it, elena.michellini@unipr.it*

^b *Department of Civil and Environmental Engineering, Politecnico di Milano, Piazza L.
da Vinci 32, 20133 Milano, Italy, gianpaolo.rosati@polimi.it*

* Corresponding author. Tel. +39 0521 905943; fax +39 0521 905924.

E-mail address: daniele.ferretti@unipr.it (D. Ferretti).

ABSTRACT

This paper aims to provide a mechanical characterization of autoclaved aerated concrete (AAC) masonry with thin bed joints subjected to in-plane loading. To this purpose, a detailed experimental program has been carried out on masonry beams subjected to bending and masonry panels subjected to uniaxial and biaxial loads. The obtained results have highlighted an almost isotropic behavior of the material. The collected data have been applied to calibrate a well-known numerical macro-model available in the technical literature for the analysis of classical masonry structures. The effectiveness of the proposed procedure has been finally verified by simulating the

23 *experimental behavior of a full-scale AAC bearing wall, through nonlinear finite*
24 *element analysis.*

25

26 **KEYWORDS**

27 AAC; thin bed masonry; experimental tests; constitutive model; mechanical properties;
28 finite element analysis.

29

1. INTRODUCTION

In recent years, the increasing demand for flexibility, comfort and energy saving in residential and industrial buildings has led both designers and manufactures to adopt new constructive systems, like Autoclaved Aerated Concrete (AAC) masonry.

AAC is a lightweight cementitious product of calcium silicate hydrates, whose low density is obtained by the presence of air bubbles in the matrix – thanks to the addition of aluminum powder in the mixture during the liquid or plastic phase – to produce a cellular structure [1]. Therefore, it offers excellent sound and thermal insulation properties [2, 3], which have led in the past decades to an increasing use of this material for non-structural applications, especially cladding and infill panels. Anyway, AAC is also characterized by a good mechanical strength and fire-resistance (due to its incombustible nature) that make it suitable for the realization of masonry bearing walls of low-to-medium rise buildings, even in seismic zones [3-10]. Compared with conventional concrete (including concrete made with lightweight aggregates), AAC has typically a lower density (which in turn reduces the seismic inertial forces acting on the structure), ranging from one-sixth to one-third, and by a lower compressive strength, which is almost reduced in the same ratio. The tendency to absorb water, related to the porous structure of the material, can further reduce its structural performances [11]; consequently, specific construction details can be required in order to achieve a satisfactory static behavior.

Since the aforementioned peculiarities make AAC different from conventional masonry materials, it is of fundamental importance to provide a detailed experimental characterization of its mechanical behavior. Test results allow indeed to calibrate sophisticated numerical models to be used in structural analyses, both for the design of

new structures and for the assessment/retrofit of existing ones [12].

As known, masonry assemblages such as shear walls, infill walls in framed construction or walls supported on beams are generally subjected to a biaxial state of stress, due to the presence of normal stresses parallel and perpendicular to the bed joints, as well as of shear stresses along the joints themselves. Moreover, unreinforced conventional masonry generally exhibits anisotropic properties due to its composite structure, with mortar joints acting as planes of weakness. Therefore, its failure cannot be described solely in terms of the two principal stresses, but a third variable – related to bed joint orientation – must be also considered. For these reasons, several researches in the past focused their attention on the experimental determination of reliable parameters of masonry strength, as well as on the development of failure criteria for masonry elements subjected to in-plane loading (e.g. [13-16]). One of the most complete experimental campaigns relative to masonry subjected to proportional biaxial loading was carried out by Page [17, 18]. These tests were performed on half-scale square panels made of solid clay units to investigate the influence exerted on failure mode and strength by bed joint orientation (with respect to the vertical principal stress direction), as well as by the applied principal stress ratio. Based on these experimental data, biaxial failure surfaces were first derived in terms of the two principal stresses and their orientation to bed joints ([17], [18]) and subsequently in terms of the stress system related to the direction of the joints [19], which is better suited for finite element modeling. Moreover, the same test results were also used in [20] to determine macroscopic elastic and non-linear stress-strain relations. However, it is worth noticing that the strength envelope obtained by Page is of limited applicability for other types of masonry, characterized by different materials, unit shapes and/or geometry. For

example, the influence of joint orientation was found to be less significant for grouted concrete masonry, whose experimental behavior under biaxial stresses seems to be essentially isotropic [21]. Further experimental investigations were also carried out on masonry panels subjected to in-plane forces, by considering different unit geometries and materials (concrete blocks, calcium-silicate blocks and clay bricks [22], or grouted unreinforced brick masonry [23]), so as to define suitable failure criteria.

It should be also remarked that the results provided from the abovementioned experimental programs could be hardly extended to AAC masonry, also because this latter belongs to “thin bed masonry” typology. The units are indeed connected together through thin glue layers, with thickness usually ranging between 0.5 and 3 mm. Researches carried out on thin bed masonry (among others, e.g. [24-27]) have shown that joint thickness significantly affects masonry behavior. As an example, the compressive strength of thin bed masonry is higher with respect to conventional masonry, since it tends to approach the strength of the blocks. Moreover, its shear and flexural strengths are not significantly affected by the interface bond behavior and therefore thin bed masonry performs more similarly to a continuum under loading, without excessive localization of the failure path along the joints. Biaxial compression tests carried out by Vermeltfoort [28] on thin bed masonry panels with different joint orientations showed that their failure mechanism was characterized by the three following phenomena: spalling of the units with fragments of approximately 20 mm, vertical splitting, and bending of the sample.

It is not clear if AAC masonry displays the same behavior. The most of the experimental programs carried out in recent years on this specific type of masonry were indeed mainly focused on the assessment of its seismic performances and were devoted

to the development of seismic design provisions to be included in Design Codes (among others, e.g. [8]-[10], [29]-[31]).

Aim of this research work is to provide a complete description of AAC masonry behavior under in-plane static loading, with particular attention to the softening regime. To the purpose, several experimental tests are performed on both AAC masonry panels and beams, so as to characterize masonry behavior under uniaxial and biaxial compression, flexure and shear, determining not only its elastic parameters and strength values, but also the fracture energies in tension and compression. The collected experimental data can be useful in the calibration of suitable numerical models; as an example, in this work an anisotropic nonlinear constitutive model, well-known in the technical literature for FE analysis of ordinary masonry structures [32-34], is adapted to AAC masonry elements. The so calibrated model is subsequently validated by performing a nonlinear FE analysis on a full-scale AAC masonry wall subjected to a pushover test [31].

2. EXPERIMENTAL PROGRAM ON AAC MASONRY ELEMENTS

The performed experimental program consisted in 33 tests on AAC masonry elements with thin bed joints. A general view of some of the assembled specimens before testing is shown in Figure 1.

In order to characterize the material behavior in compression, several monotonic uniaxial and biaxial tests were performed on small-scale masonry panels, by varying the bed joint orientation with respect to the horizontal axis. Some of the uniaxial tests were carried out under displacement control to obtain the complete stress-strain curve and the

corresponding fracture energy in compression.



Figure 1. General view of some of the AAC masonry specimens tested during the experimental program.

Due to the limited features of the universal testing machines at our disposal, tensile behavior of AAC masonry was instead investigated indirectly, by performing three-point bending tests on small-scale masonry beams. In this case, only two angles of inclination between the bed joints and the horizontal axis were considered (namely 0° and 90°). For each examined typology, two beams were provided of a central notch to guide crack formation and were tested under crack mouth opening displacement (CMOD) control, so obtaining the complete load-deflection response and the corresponding fracture energy in tension. Finally, two small masonry panels were subjected to diagonal compression tests.

2.1 Description of test specimens

All the specimens were prepared by using masonry-type AAC units directly provided by the Manufacturer. It is worth noticing that AAC units are commonly produced in different sizes that may reach $625 \times 250 \times 200$ mm; in this last case, masonry panels including a representative number of head and bed joints would be huge and some problems may arise to test them into the frame of a universal testing machine.

However, considering that the dimensions of the units available on the market are variable, in the present work it has been preferred to employ non-standard small size bricks, with nominal dimensions equal to 250×50×100 mm. In this way, it has been possible to keep the specimen size small, while having at the same time an adequate number of head and bed joints, so emphasizing their influence on masonry global behavior and increasing possible anisotropic effects. Therefore, the behavior of structural elements realized with larger units and a more limited number of joints should lie between the two “limit cases” of homogeneous material (previously investigated by the same Authors in [35]) and the here investigated masonry formed by small units. In any case, experimental evidences have shown that the use of scaled bricks does not seem to alter substantially the results, as will be discussed in more details in the forthcoming Sections.

A deep characterization of the raw autoclaved aerated concrete adopted for the realization of units can be found in [35]. Its main mechanical characteristics were: average density $\rho_b = 550 \text{ kg/m}^3$, average compressive strength $f_b = 3.1 \text{ MPa}$ (as determined on cubes with an edge length of 100 mm), average modulus of rupture $f_{t,b} = 0.6 \text{ MPa}$, and elastic modulus $E_b = 1320 \text{ MPa}$.

Units were assembled by using a specific cementitious grey glue produced by the same Manufacturer, mainly composed of Portland cement, silica sand and specific additives, with a water dosage equal to 24% in weight. This grey glue was a guaranteed performance mortar characterized by the following main properties: average density $\rho_g = 1300 \text{ kg/m}^3$, average compressive strength of cylindrical specimens $f_g = 7 \text{ MPa}$ (it was instead equal to 6 MPa when determined on 40×40×160 mm prisms), average modulus of rupture $f_{t,g} = 2.7 \text{ MPa}$, elastic modulus $E_g = 5300 \text{ MPa}$. The nominal

thickness of head and bed joints was equal to 1.5 mm.

To allow a complete drying of the glue and the reaching of stationary moisture conditions, all the specimens were stored in laboratory for more than three months. At time of test execution, all samples were characterized by an average moisture content approximately equal to 2.4% and by an average density $\rho = 550 \text{ kg/m}^3$.

As already mentioned, uniaxial and biaxial compression tests were performed on 23 small-scale masonry panels, with length of 625 mm, thickness equal to 100 mm and height equal to 750 mm. Two additional uniaxial tests were performed on smaller square panels with an edge length of 250 mm, characterized by the same thickness. This last specimen geometry was also adopted for the two diagonal compression tests. Flexural tests were instead carried out on six small-scale masonry beams with length of 625 mm, thickness equal to 100 mm and height equal to 250 mm. Further details about sample characteristics and adopted test arrangements are reported in the following Sections.

2.2 Characterization of AAC masonry panels in compression

2.2.1 Uniaxial compression tests

Uniaxial compression tests were performed on 17 small-scale masonry panels (Figure 2a). In order to study the influence exerted by the geometrical arrangement of units and joints on masonry compressive strength, 5 specimen typologies, characterized by a different inclination θ of glue beds – equal to 0° , 22° , 45° , 68° and 90° with respect to the horizontal direction – were considered, as depicted in Figure 2a. The same Figure also provides specimen nominal dimensions, as well as their denomination, which is composed by the acronym PMC (which stands for Panel Masonry Compression),

followed by two digits, the first one representing the angle of inclination of glue beds and the second one (in brackets) the total number of tested samples belonging to a considered typology.

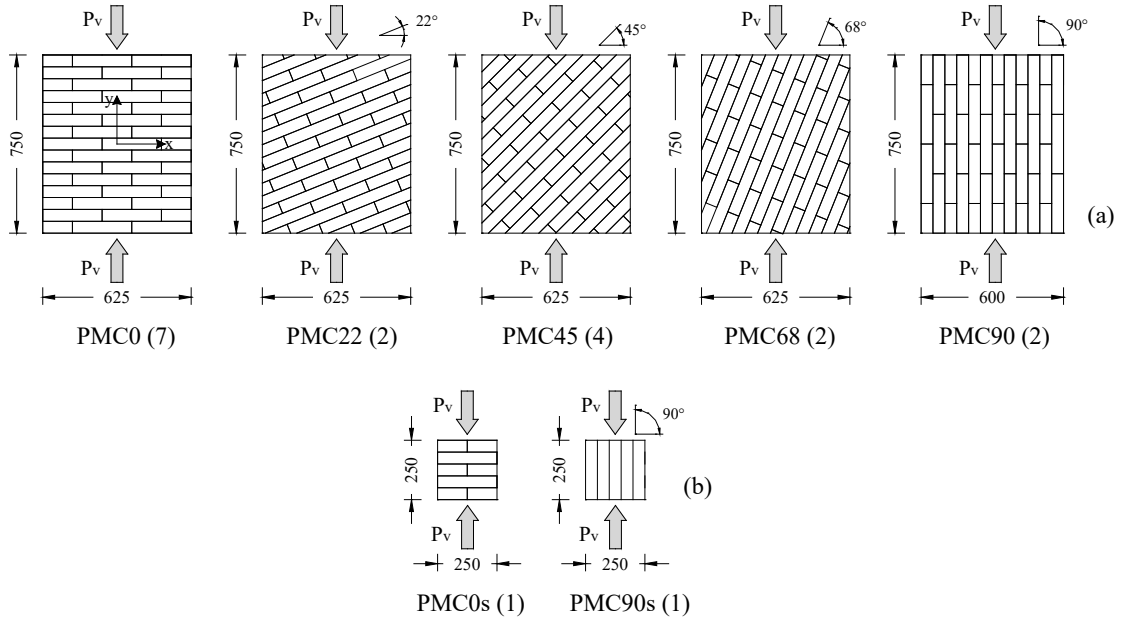


Figure 2. Sketch of uniaxial compression tests on masonry panels (a) PMC and (b) PMCs (characterized by reduced dimensions).

A larger part of this experimental program (15 samples) was carried out at the Laboratory of the AAC Manufacturer Company, by using a Metrocom PV50 press working under loading control, with a capacity of the hydraulic actuator equal to 5000 kN [36]. The adopted test arrangement is shown in Figure 3; in order to apply a distributed load, a 650 mm long steel rigid beam with I-section was placed on the top of the sample. Panel surfaces were preliminary flattened by sandpaper to eliminate any irregularity and thereby ensure a complete contact between the specimen itself and the testing apparatus. Furthermore, two overlapping Teflon sheets were interposed to minimize the confinement effect due to friction and apply a uniform state of stress. The most of these tests simply provided the uniaxial compressive strengths f_{mx} , f_{my} in the two

masonry principal directions (respectively parallel, x , and perpendicular, y , to glue beds). Three of these 15 samples – denoted as PMC0-2, PMC0-3, and PMC90-1 – were also instrumented with 6 linear variable displacement transducers (LVDTs) aligned along x and y directions on the two opposite panel faces, as shown in Figure 3b. The LVDTs were installed to measure vertical and horizontal strains (ε_v and ε_h), so allowing the evaluation of the elastic moduli E_x and E_y in the two masonry principal directions, as well as the Poisson coefficient ν . Moreover, it was also possible to follow the initial part of the softening branch by performing a gradual unloading of the specimen after the reaching of the peak load.



Figure 3. General setup of uniaxial compression tests performed under loading control: (a) not instrumented and (b) instrumented small-scale masonry panels (PMC).

The remaining two samples (respectively indicated as PMC0-7 and PMC90-2 according to Figure 2a) were tested at the Materials and Structures Laboratory of Milan Polytechnic University, by using a 1000 kN Schenck press working under displacement control (Figure 4a). Two 650 mm long steel rigid beams with I-section were placed on the top and bottom bases of the specimen, by interposing two thin Teflon sheets in order to reduce friction. All samples were instrumented with 6 LVDTs aligned along x and y

directions on the two opposite panel faces, as shown in Figure 4a. These tests provided the complete stress-strain curve for the material in compression.

The so obtained results were subsequently integrated by testing two additional smaller panels (Figure 2b), respectively characterized by horizontal (PMCs0) and vertical (PMCs90) glue beds.

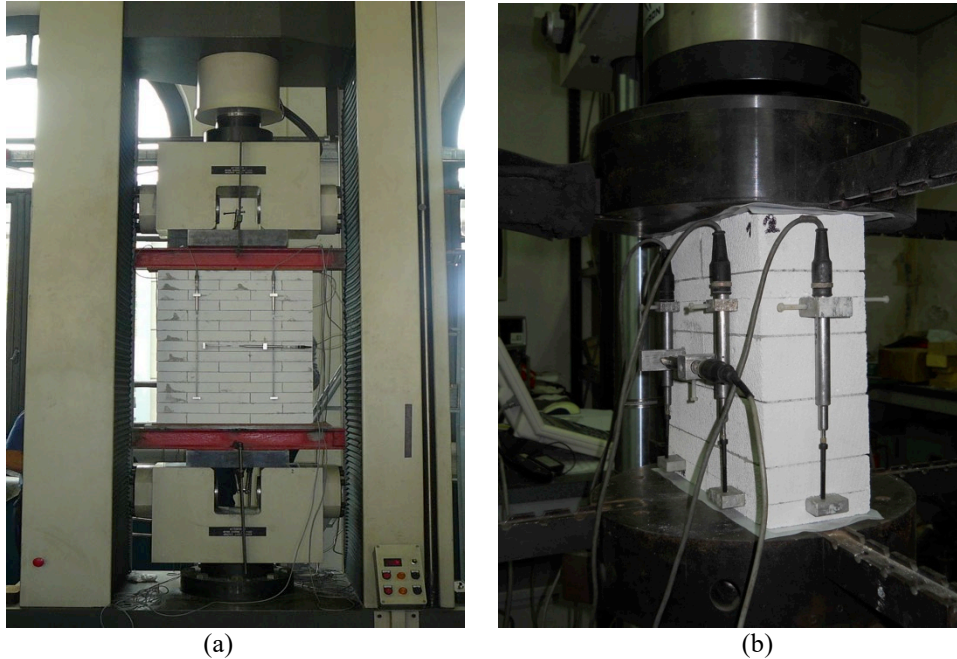


Figure 4. General setup of uniaxial compression tests performed under displacement control: (a) small-scale masonry panels (PMC) and (b) square specimens with reduced dimensions (PMCs).

In this last case, a 100 kN Instron 8862 press working under displacement control was used and the samples were still instrumented with 6 LVDTs aligned along x and y directions on the two opposite panel faces, with two further vertical LVDTs in the thickness (Figure 4b). These two additional specimens were realized in order to achieve a better description of the post-peak response, since bigger panels displayed local failures that determined in some cases sudden jumps in the softening branch of the stress-strain curve.

The main results of the above-described tests are summarized in Table 1 in terms

of experimental failure load $P_{v,u}$ and corresponding vertical compressive stress σ_v for each tested panel.

Sample	#	Test control	L (mm)	t (mm)	H (mm)	$P_{v,u}$ (kN)	σ_v (MPa)	σ_x (MPa)	σ_y (MPa)	τ_{xy} (MPa)
PMC0	1	LC	622.00	100.90	740.00	160.82	-2.56	0.00	-2.56	0.00
PMC0	2	LC	621.00	99.50	746.00	151.27	-2.45	0.00	-2.45	0.00
PMC0	3	LC	621.00	99.11	745.00	167.50	-2.72	0.00	-2.72	0.00
PMC0	4	LC	622.00	99.86	744.00	140.75	-2.27	0.00	-2.27	0.00
PMC0	5	LC	623.00	99.71	745.00	171.33	-2.76	0.00	-2.76	0.00
PMC0	6	LC	623.00	99.87	747.00	151.27	-2.43	0.00	-2.43	0.00
PMC0	7	DC	623.00	100.00	756.00	172.86	-2.77	0.00	-2.77	0.00
PMCs0	1	DC	240.00	100.00	250.00	67.14	-2.80	0.00	-2.80	0.00
PMC90	1	LC	610.00	100.00	741.00	156.00	-2.56	-2.56	0.00	0.00
PMC90	2	DC	610.00	100.00	740.00	143.57	-2.35	-2.35	0.00	0.00
PMCs90	1	DC	250.00	100.00	246.00	72.03	-2.88	-2.88	0.00	0.00
PMC22	1	LC	627.00	100.00	751.00	141.84	-2.26	-0.32	-1.94	0.79
PMC22	2	LC	625.00	100.00	749.00	143.59	-2.30	-0.32	-1.98	0.80
PMC45	1	LC	627.00	100.00	747.00	133.08	-2.12	-1.06	-1.06	1.06
PMC45	2	LC	625.00	100.00	748.00	137.46	-2.20	-1.10	-1.10	1.10
PMC45	3	LC	623.00	99.50	749.00	139.21	-2.25	-1.12	-1.12	1.12
PMC45	4	LC	625.00	100.00	748.00	139.21	-2.23	-1.11	-1.11	1.11
PMC68	1	LC	624.00	100.00	748.00	134.83	-2.16	-1.86	-0.30	0.75
PMC68	2	LC	625.00	100.00	748.00	128.70	-2.06	-1.77	-0.29	0.72

LC = loading control

DC = displacement control

Table 1. Uniaxial compression tests on AAC masonry panels (PMC and PMCs): effective dimensions of the specimens and experimental failure loads.

The same Table also reports the total stress state related to bed joints σ_x , σ_y and τ_{xy} (being x , y the directions respectively parallel and perpendicular to bed joints, as depicted in Figure 2a), which has been subsequently deduced by using the following standard relations [19]:

$$\sigma_x = \frac{\sigma_v + \sigma_h}{2} - \frac{\sigma_v - \sigma_h}{2} \cos(2\theta)$$

$$\sigma_y = \frac{\sigma_v + \sigma_h}{2} + \frac{\sigma_v - \sigma_h}{2} \cos(2\theta) \quad (1)$$

$$\tau_{xy} = \frac{\sigma_v - \sigma_h}{2} \sin(2\theta).$$

These equations, that are valid for a general biaxial state of stress (being σ_v and σ_h the

vertical and horizontal principal stresses, respectively, and θ the angle between bed joints and the horizontal axis), have been here applied to the uniaxial case by simply posing $\sigma_h = 0$. Table 1 also indicates the effective specimen dimensions (L , t , H), as well as the adopted type of testing, that is to say under displacement or loading control (respectively indicated as DC and LC).

Experimental results highlighted that the compressive strengths in the two principal directions x - y – respectively obtained as the average peak stress values σ_v for PMC90 and PMC0 samples – were almost equal to each other ($f_{mx} \approx f_{my} \approx 2.60$ MPa). A slight reduction of masonry compressive strength - ranging between 13 and 24% - was instead observed for other angles of bed joints (that is $\theta = 22^\circ, 45^\circ, 68^\circ$).

Based on the results of this investigation, it seems that bed joint orientation exerts only a limited influence on the compressive behavior of tested panels, as also reported in the literature for other types of thin bed masonry [25]. This is mainly due to the isotropic behavior of AAC units (which do not have internal perforations), as well as to the presence of thin glue joints with a relatively high strength.

Moreover, AAC masonry compressive strength in the two principal directions x - y appears to be only slightly lower with respect to that of the raw material, as determined on AAC prisms and cubes sawed from some of the tested masonry specimens (Figure 5a). The first ones, characterized by a 40 mm square basis and 80 mm height, provided indeed an average uniaxial compressive strength approximately equal to $f_{AAC} = 2.8$ MPa, while for 40 mm side cubes a value of $f_{AAC,cube} = 3.1$ MPa was found. These values were almost coincident with those provided from standard tests previously carried out on the adopted raw material (see [35] for further details), as well as with those available in the technical literature for a material with similar density and moisture content [5-6].

Anyway, it should be kept in mind that AAC compressive strength depends on the geometry and dimensions of tested blocks. Compression tests performed on raw-AAC panels with nominal dimensions equal to those of masonry ones (625 x 750 x 100 mm, Figure 5b) and produced by the same Manufacturer provided indeed an average compressive strength $f_c = 2.4$ MPa, which is comparable to that obtained from masonry specimens.

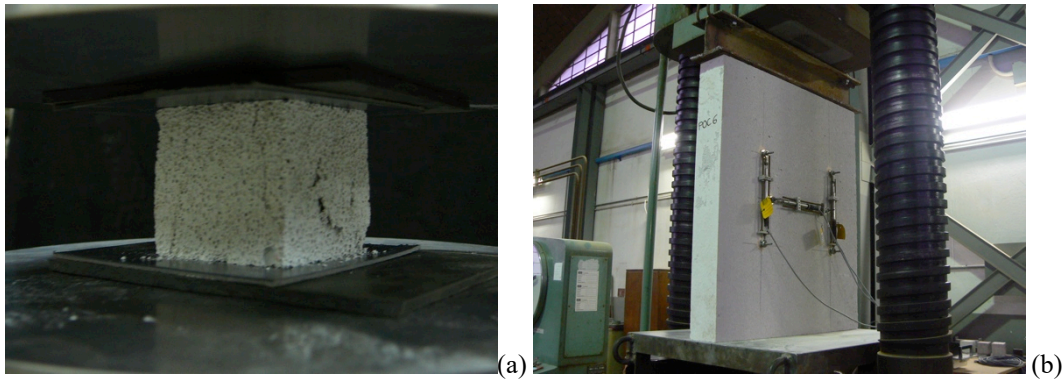


Figure 5. Uniaxial compression tests on homogeneous AAC samples: (a) cubes with an edge length of 40 mm and (b) panels with the same geometry and dimensions of PMC masonry ones.

This result is not surprising when considering both the high strength of the cementitious glue and the relatively small size of adopted units, which allowed a random redistribution of the defects in the tested panel. In homogeneous samples, failure was instead mainly localized near the weaker edge, related to the expansion process. Moreover, at time of test execution, masonry samples were characterized by a slightly lower moisture content with respect to homogeneous ones ([35]).

Masonry elastic properties are summarized in Table 2. Elastic moduli were determined as the chord slope of the stress - vertical strain curve (within a stress interval ranging from $0.05 \sigma_v$ and $0.33 \sigma_v$), so obtaining an average value respectively equal to $E_x = 1700$ MPa for PMC90 samples (with vertical glue beds) and $E_y = 1400$ MPa for

PMC0 samples (with horizontal glue beds). This last value was calculated by discarding the result relative to PMCs0 sample, which was characterized by an anomalous more rigid behavior compared to the other ones belonging to the same typology. The obtained values are of the same order of magnitude as the ones provided by Manufacturer certifications and technical sheets, which range between 1400 MPa and 1750 MPa (referred to a masonry with horizontal glue beds). Poisson coefficient was instead evaluated as the ratio between horizontal and vertical strains ($\varepsilon_h / \varepsilon_v$), obtaining an average value almost equal to $\nu \cong 0.30$ in both the two main directions. It can be observed that the so determined elastic properties are similar, even if not identical, to those previously derived on homogeneous panels, which were respectively equal to $E = 1352$ MPa and $\nu = 0.38$, as reported in [35].

Table 2 also summarizes the strains values corresponding to peak stresses, which were respectively equal, on average, to $\varepsilon_{px} = 1.8\text{‰}$ and $\varepsilon_{py} = 2.2\text{‰}$.

Sample	#	Test control	E_x (MPa)	E_y (MPa)	ν (MPa)	ε_{px} (‰)	ε_{py} (‰)
PMC0	2	LC		1417	0.32		2.00
PMC0	3	LC		1392	0.38		2.20
PMC0	7	DC		1346	0.29		2.40
PMCs0	1	DC		1737	0.35		1.68
PMC90	1	LC	1653		0.29	1.90	
PMC90	2	DC	1713		0.26	1.50	
PMCs90	1	DC	1719		0.25	2.10	

LC = loading control
DC = displacement control

Table 2. Uniaxial compression tests on AAC masonry panels (PMC and PMCs): elastic moduli E_x , E_y , Poisson ratio ν and compressive peak strains ε_{px} and ε_{py} .

Finally, the observed crack patterns at failure are shown in Figure 6. Depending on the orientation of the bed joints to the applied load, failure mainly occurred by cracking and sliding in the bed and/or head joints, or in a combined mechanisms

involving cracking in both units and joints. As can be seen from Figure 6a-b, for both PMC0 and PMC22 panels a major crack developed in the direction perpendicular to bed joints, alternatively crossing AAC blocks and thin glue layers. On the contrary, in PMC90 and PMC68 samples (Figure 6d-e), cracks mainly developed along glue beds, while for PMC45 ones (Figure 6c) the observed failure mode was less defined, with diagonal cracks spreading at the same time both in glue beds and AAC blocks.

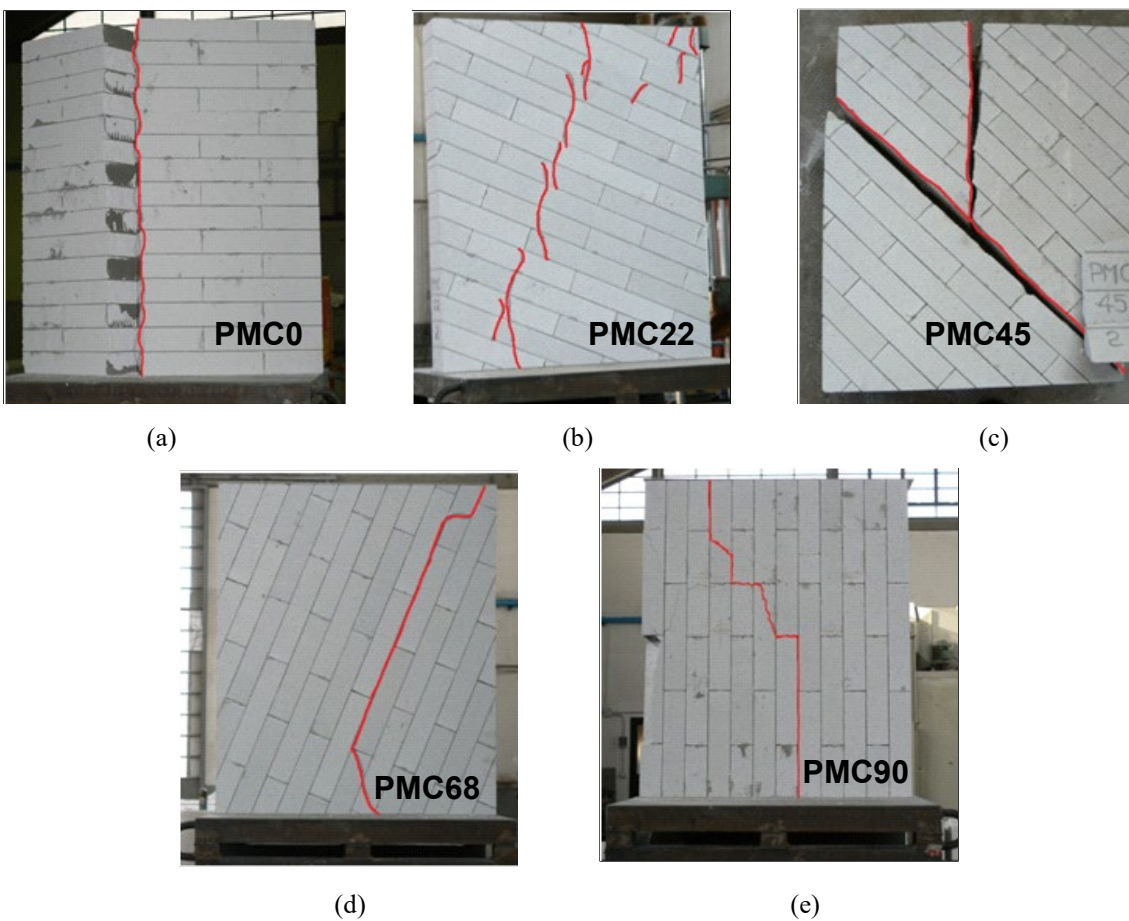


Figure 6. Uniaxial compression tests on AAC masonry panels (PMC): observed crack patterns at failure as function of bed joint inclination.

2.2.2 Biaxial compression tests

Biaxial compression tests were carried out on the same panel typologies already

subjected to uniaxial compression, as depicted in Figure 7a. As can be seen from the
 same Figure, these panels were named PMB (which stands for Panel Masonry Biaxial
 compression), followed by two digits, the first one representing the angle of inclination
 of glue beds with respect to the horizontal axis and the second one (in brackets) the total
 number of tested samples belonging to a considered typology. In this case, three
 different inclinations of bed joints were considered (0° , 22° , and 45°) for a total of 6
 samples, two for each typology. Since equal compressive forces were applied in the two
 principal directions, 68° and 90° inclinations were indeed coincident with 22° and 0° .

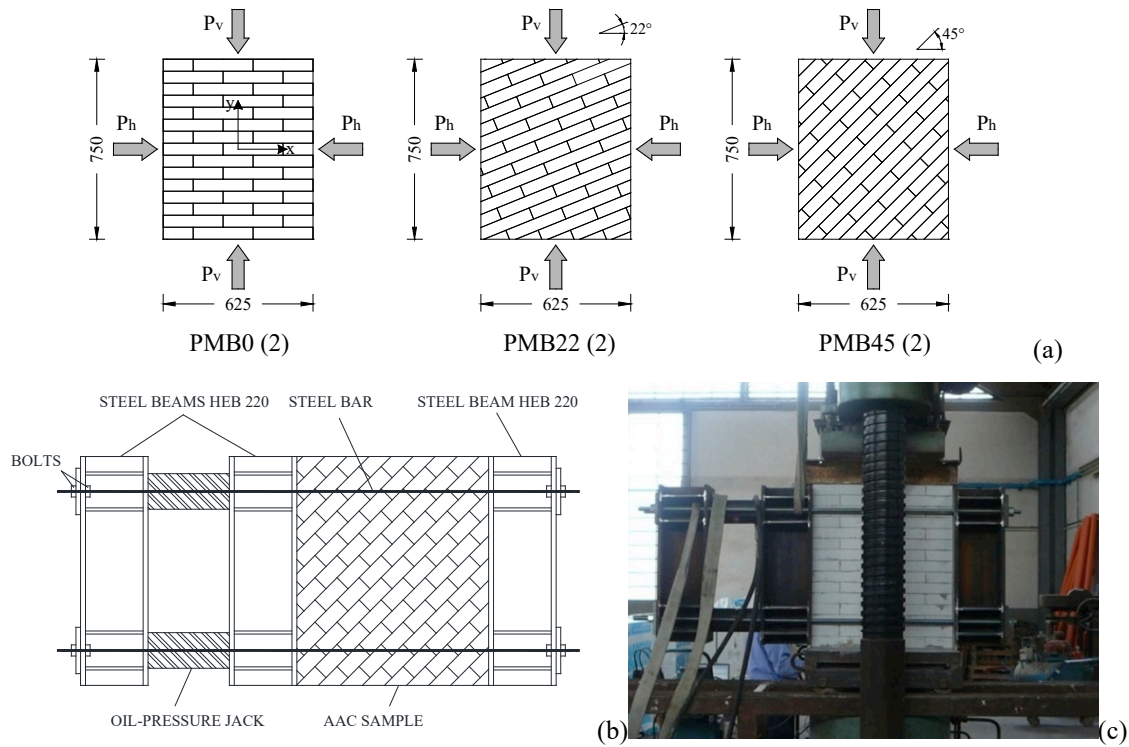


Figure 7. (a) Sketch of biaxial compression tests on masonry panels (PMB); (b) sketch and (c) general view of the adopted setup.

Vertical load P_v was applied by using the same Metrocom PV50 press already
 used for uniaxial compression tests, by adopting a similar loading arrangement (with a
 steel rigid beam on the top of the sample and thin Teflon layers interposed between the

sample and the loading apparatus). Lateral confinement P_h was instead applied by adopting the device depicted in Figure 7b-c, formed by a system of steel rigid beams connected together through steel ribbed bars. These beams were placed on the sides of the AAC sample (by interposing the usual thin Teflon layers) and were used as contrast for two oil-pressure jacks, aligned in the horizontal direction. Biaxial tests were performed under loading control by monitoring that the same value of vertical and horizontal pressure was simultaneously applied on sample surfaces (the two loading devices were indeed not directly connected to each other). In this case, none of the specimen was instrumented.

The main results of the above described tests are summarized in Table 3, in terms of experimental failure loads $P_{v,u}$ and $P_{h,u}$, as well as corresponding stresses σ_v and σ_h . From these values, the total stress state related to bed joints σ_x , σ_y and τ_{xy} has been also determined (being x , y the directions respectively parallel and perpendicular to bed joints, as depicted in Figure 7a), by still applying Equations 1. The obtained results confirm that the bed joint angle exerts only a limited influence on the strength of masonry; moreover, the biaxial strength value is substantially comparable with the uniaxial one. Table 3 also reports the effective specimen dimensions (L , t , H).

Sample	#	Test control	L (mm)	t (mm)	H (mm)	$P_{v,u}$ (kN)	σ_v (MPa)	$P_{h,u}$ (kN)	σ_h (MPa)	σ_x (MPa)	σ_y (MPa)	τ_{xy} (MPa)
PMB0	1	LC	624	100	761	138.09	-2.21	165.52	-2.18	-2.18	-2.21	0.00
PMB0	2	LC	623	100	760	143.10	-2.30	171.61	-2.26	-2.26	-2.30	0.00
PMB22	1	LC	626	100	749	137.66	-2.20	159.54	-2.13	-2.14	-2.19	0.02
PMB22	2	LC	625	100	750	146.19	-2.34	173.48	-2.31	-2.32	-2.34	0.01
PMB45	1	LC	626	100	748	124.51	-1.99	142.12	-1.90	-1.95	-1.95	0.04
PMB45	2	LC	624	100	748	137.22	-2.20	161.57	-2.16	-2.18	-2.18	0.02

LC = loading control

DC = displacement control

Table 3. Biaxial compression tests on AAC masonry panels (PMB): effective dimensions of the specimens and experimental failure loads.

The observed crack patterns at failure are depicted in Figure 8. As can be seen, all panels showed the same failure mode, characterized by an out-of-plane expansion in the unconfined direction, regardless of bed joint orientation. Spalling of small masonry fragments was also observed.

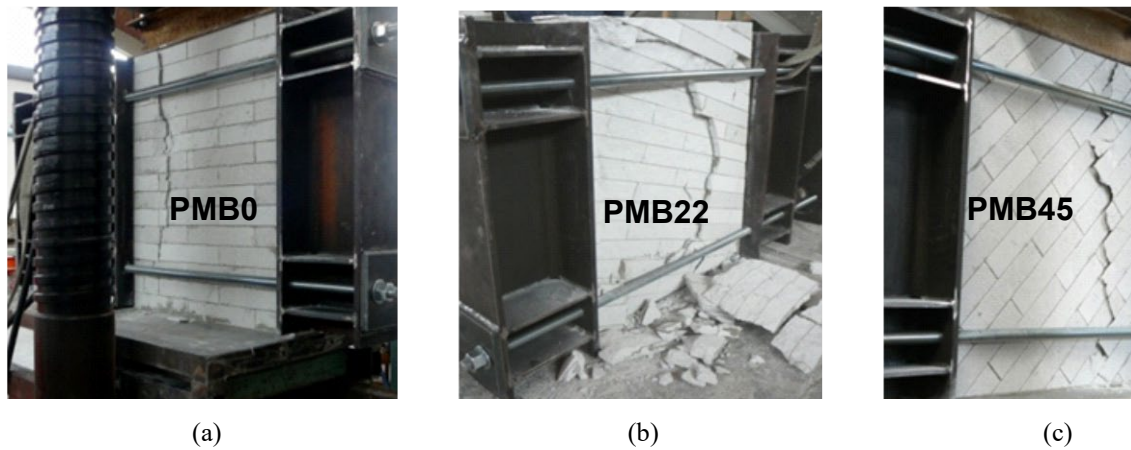


Figure 8. Biaxial compression tests on AAC masonry panels (PMB): observed crack patterns at failure as function of bed joint inclination.

2.3 Characterization of AAC masonry beams in flexure

Three-point bending tests were performed on six AAC small-scale masonry beams, with nominal dimensions equal to 625 x 250 x 100 mm (Figure 9).

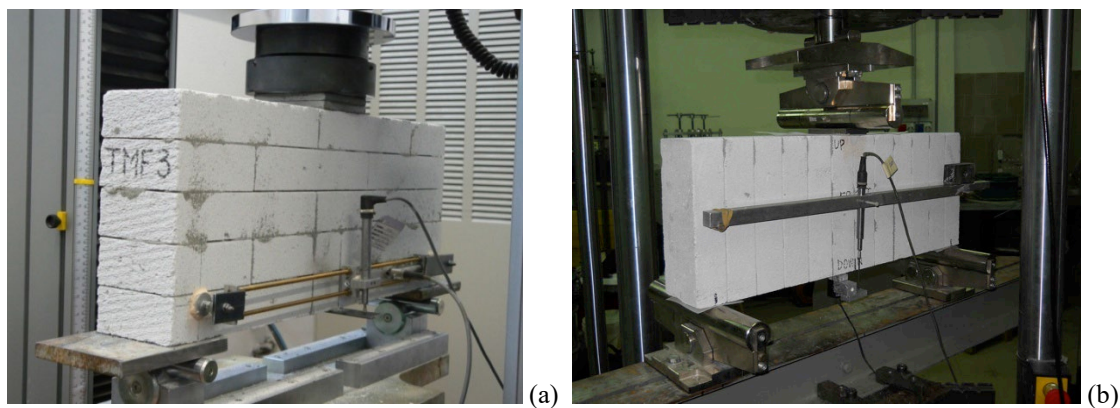


Figure 9. Three-point bending tests on AAC masonry beams BMF (a) without and (b) with notch: adopted setup.

The main characteristics of the tested samples, as well as the adopted nomenclature are summarized in Figure 10. In this case, the acronym BMF (which stands for Beam Masonry Flexure) has been adopted, followed by a number representing the angle of inclination of bed joints with respect to the horizontal axis; a further digit (in brackets) indicates the number of tested specimens belonging to the same typology. In more detail, 4 specimens BMF0 (with horizontal bed joints) and 2 specimens BMF90 (with vertical bed joints) were realized; for each typology, 2 beams were provided of a central notch, so as to guide crack formation. It should be here observed that the two BMF90 specimens were characterized by different effective lengths and net spans, as highlighted in Table 4. The first sample was indeed formed by an odd number of units (13), so having the notch placed at half-width of the central brick line; however, the experimental failure was localized in correspondence of one of the adjacent glue joints. For this reason, the other specimen was realized with an even number of units (one less than sample BMF90-1), to place the notch exactly in correspondence of the glue joint.

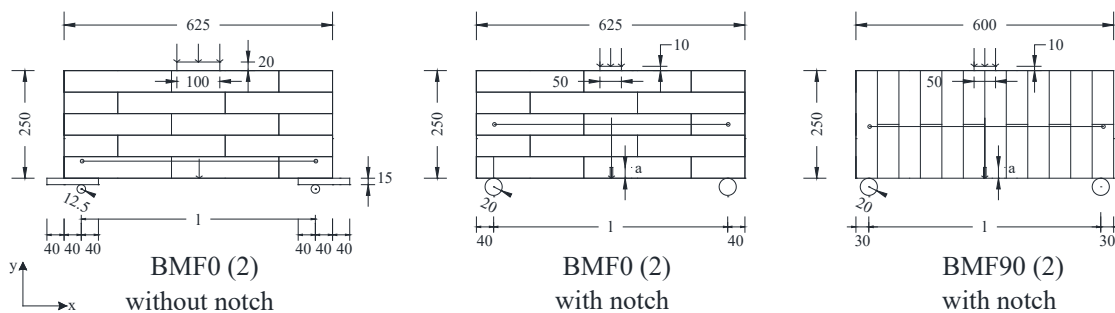


Figure 10. Sketch of three-point bending tests on AAC masonry beams BMF: (a) unnotched specimens BMF0; specimens (b) BMF0 and (c) BMF90 with a central notch.

The two unnotched specimens were tested at the Laboratory of the AAC Manufacturer Company, by using an Instron 5882 press working under loading control,

with a loading rate of about 1 kN/min (Figure 9a). The 4 notched samples were instead tested at the Materials and Structures Laboratory of Milan Polytechnic University, by using an Instron 8862 press working under CMOD control, with a loading rate of 1 $\mu\text{m}/\text{min}$ (Figure 9b). All the specimens were instrumented with a LVDT properly fixed on a bar installed over the two supports, in order to monitor the true midspan deflection during test execution (Figure 9 a-b).

The performed tests provided the failure load in flexure $P_{u,fl}$ for the two investigated bed joint angles, as reported in Table 4.

Sample #	Test control	L (mm)	t (mm)	H (mm)	a (mm)	l (mm)	$P_{u,fl}$ (kN)	f'_{tx} (MPa)	G_{fx} (N/mm)	f'_{ty} (MPa)	G_{fy} (N/mm)
BMF0 1	LC	625.4	100.6	251.2	0.0	545.4	2.67	0.34	-	-	-
BMF0 2	LC	624.2	100.1	251.7	0.0	544.2	2.94	0.38	-	-	-
BMF0 3	DC	625.0	100.0	250.0	37.5	545.0	2.34	0.42	6.4E-03	-	-
BMF0 4	DC	626.0	100.0	258.0	25.0	546.0	2.27	0.34	7.8E-03	-	-
BMF90 1	DC	660.0	100.0	250.0	12.5	600.0	2.56	-	-	0.37	4.5E-03
BMF90 2	DC	610.0	100.0	240.0	24.0	550.0	1.31	-	-	0.23	5.8E-03

LC = loading control

DC = displacement control

Table 4. Three-point bending tests on AAC masonry beams (BMF): effective dimensions of the specimens, experimental failure loads, indirect tensile strengths and fracture energies in tension.

The corresponding flexural tensile strengths (moduli of rupture) in the two examined directions were subsequently determined through a linear elastic FE inverse analysis, so obtaining an average value respectively equal to $f'_{tx} = 0.37$ MPa and $f'_{ty} = 0.30$ MPa. Moreover, tests carried out under CMOD control allowed the determination of the complete post-peak load-deflection response and consequently of the two average fracture energies in tension, respectively equal to $G_{fx} = 7.10 \cdot 10^{-3}$ N/mm and $G_{fy} = 5.15 \cdot 10^{-3}$ N/mm. The obtained results, as well as the effective sample dimensions, are reported in detail in Table 4. As can be seen, the first BMF90 sample provided a tensile strength comparable to that obtained for BMF0 samples, while the

second one presented a value approximately 40% lower, probably due to a not proper filling of the central glue joint.

It can be also observed that both the strength and the fracture energy of masonry samples in the two examined directions are comparable to those of the homogeneous material, as reported in the technical literature [5, 35, 37, 38].

2.4 Characterization of AAC masonry panels in diagonal compression

The characterization of AAC masonry behavior was completed through the testing of two small panels in diagonal compression, as depicted in Figure 11a-b. Those samples, named PMS (Panel Masonry Shear), were characterized by nominal dimensions equal to 250 x 250 x 100 mm. The tests were still carried out at the Materials and Structures Laboratory of Milan Polytechnic University, by using an Instron 8862 press to apply the vertical load P_v . In order to avoid the crushing of loaded angles and to obtain a uniform state of stress, thin cardboard layers were interposed between the loading platens and the sample, as shown in Figure 11b.

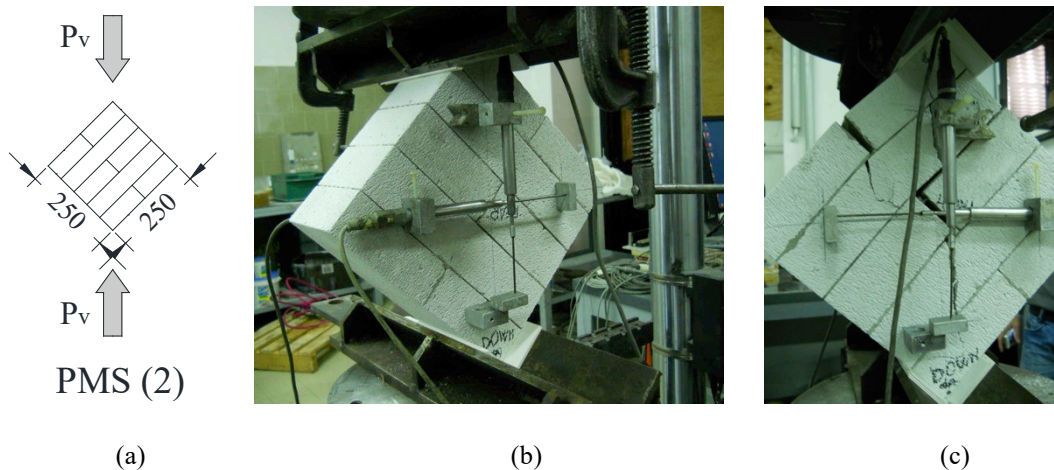


Figure 11. (a) Sketch and (b) adopted arrangement of diagonal compression tests on small AAC masonry panels PMS; (c) observed failure mode.

As can be seen from the same Figure, each sample was instrumented with 2

vertical and 2 horizontal LVDTs, so as to record panel strains with increasing loads.

The obtained results, as well as the effective sample dimensions, are summarized in Table 5, in terms of vertical load at failure P_v and corresponding masonry shear strength (under zero compressive stresses) $f_{v0} = 0.7P_v / A_n$, being A_n the net area of the panel. The latter has been evaluated as $A_n = t (H+L)/2$, where H and L are the sides of the panel and t is the thickness. As can be observed from Table 5, these values are rather high if compared to those suggested in technical Codes (e.g., [39]) or determinable with common empirical relations, such as $f_{v0} \approx 0.15 f_m$, being f_m the masonry compressive strength [40].

Sample	#	Test control	L (mm)	t (mm)	H (mm)	P_v (kN)	f_{v0} (MPa)	σ_x (MPa)	σ_y (MPa)	τ_{xy} (MPa)
PMS	1	DC	240	100	240	19.91	0.59	-0.49	-0.49	0.92
PMS	2	DC	250	100	250	25.74	0.73	-0.60	-0.60	1.14

LC = loading control

DC = displacement control

Table 5. Diagonal compression tests on small AAC masonry panels (PMS): effective dimensions of the specimens and experimental failure loads.

The same Table also reports the total stress state related to bed joints σ_x , σ_y and τ_{xy} . As concerns the observed failure modes, both the specimen presented the spreading of a main sub-vertical crack, alternatively crossing AAC blocks and glue joints (Figure 11c).

3. CALIBRATION OF A NUMERICAL MACRO-MODEL FOR AAC MASONRY BASED ON THE EXPERIMENTAL RESULTS

The described experimental results have been used for the calibration of the well-known macro-model proposed by Lourenço et al. [32-34] for the analysis of masonry structures. This model, which treats masonry as an anisotropic continuum and describes

its behavior in terms of average stresses and strains, seems an appropriate tool for simulating the behavior of AAC walls, as well as that of other types of thin bed masonry [25], due to the quite limited influence of the interface. For finite element analyses, the material model has been implemented in [41] into a computer algorithm that handles plasticity features like return mapping, corners, apex, etc. This algorithm has been here converted into a user material subroutine (UMAT) and implemented into the general purpose finite element code ABAQUS [42] to perform numerical simulations.

In the following Sections, the adopted model will be first briefly described and its calibration to the case of AAC masonry will be subsequently discussed.

3.1 Main features of the adopted macro-model

The considered model [32-34], which has been developed with reference to general plane stress conditions, represents an extension of conventional formulations for isotropic quasi-brittle materials to describe orthotropic behavior. Two different failure criteria are adopted for tension and compression, respectively “Rankine-type” and “Hill-type”, whose equations [33] are recalled in Figure 12a. As can be seen in Figure 12b, the non-linear behavior of masonry in compression $\bar{\sigma}_{ci} - \kappa_c$ (where the subscript i refers to the material axis x or y) is described through a parabolic plastic stress-strain relationship ($\bar{\sigma}_{ai} - \kappa_c$, according to Fig. 12b) until the reaching of the peak value, which is usually different in the two principal orthotropic directions x - y - namely $\bar{\sigma}_{px} = f_{mx}$ and $\bar{\sigma}_{py} = f_{my}$. After the peak, a parabolic/exponential softening branch ($\bar{\sigma}_{bi} - \kappa_c$ and $\bar{\sigma}_{di} - \kappa_c$, respectively) is adopted in both directions, characterized by different fracture energies G_{fcx} and G_{fcy} . The inelastic work $g_{fci} = G_{fci}/h$ in Figure 12 is

related to the fracture energy G_{fci} through the equivalent length h , which corresponds to a representative dimension of the mesh size (so that the obtained results are objective with regard to mesh refinement). According to [32], the compressive law shown in Figure 12b can be defined on the basis of three stresses (that is initial, mean and residual ones), which are determined as a fraction of the peak value $\bar{\sigma}_{pi} = f_{mi}$ through the following relations: $\bar{\sigma}_{ii} = 1/3 f_{mi}$, $\bar{\sigma}_{mi} = 1/2 f_{mi}$, $\bar{\sigma}_{ri} = 1/10 f_{mi}$. The equivalent plastic strain κ_p , corresponding to the peak compressive strength, is assumed to be an additional material parameter. Furthermore, in order to obtain a mesh independent energy dissipation, it should be posed [32]:

$$\kappa_{mi} = \frac{75}{67} \frac{G_{fci}}{h f_{mi}} + \kappa_p, \quad (2)$$

with the limitations reported in [32, 34].

The nonlinear behavior of masonry in tension is instead described through an exponential softening plastic stress-strain relationship $\bar{\sigma}_{ti} - \kappa_t$, with different tensile strengths (f_{tx} and f_{ty}) and fracture energies (G_{fx} and G_{fy}) in the two principal orthotropic directions (Figure 12c). The exhaustive theoretical formulation of the adopted model can be found in [32-34], to which reference is made for further details.

To be correctly calibrated, the considered model requires the knowledge of seven parameters governing material strength (respectively indicated as $f_{tx}, f_{ty}, f_{mx}, f_{my}, \alpha, \beta$ and γ), as well as five inelastic parameters governing the plastic stress-strain relationships ($G_{fx}, G_{fy}, G_{fex}, G_{fey}$ and κ_p). The first four strength properties (which represent uniaxial tensile f_{ti} and compressive f_{mi} strengths along the material axes $i = x, y$) can be determined by performing uniaxial tension and compression tests on masonry

specimens, along the two main directions respectively parallel and perpendicular to mortar beds.

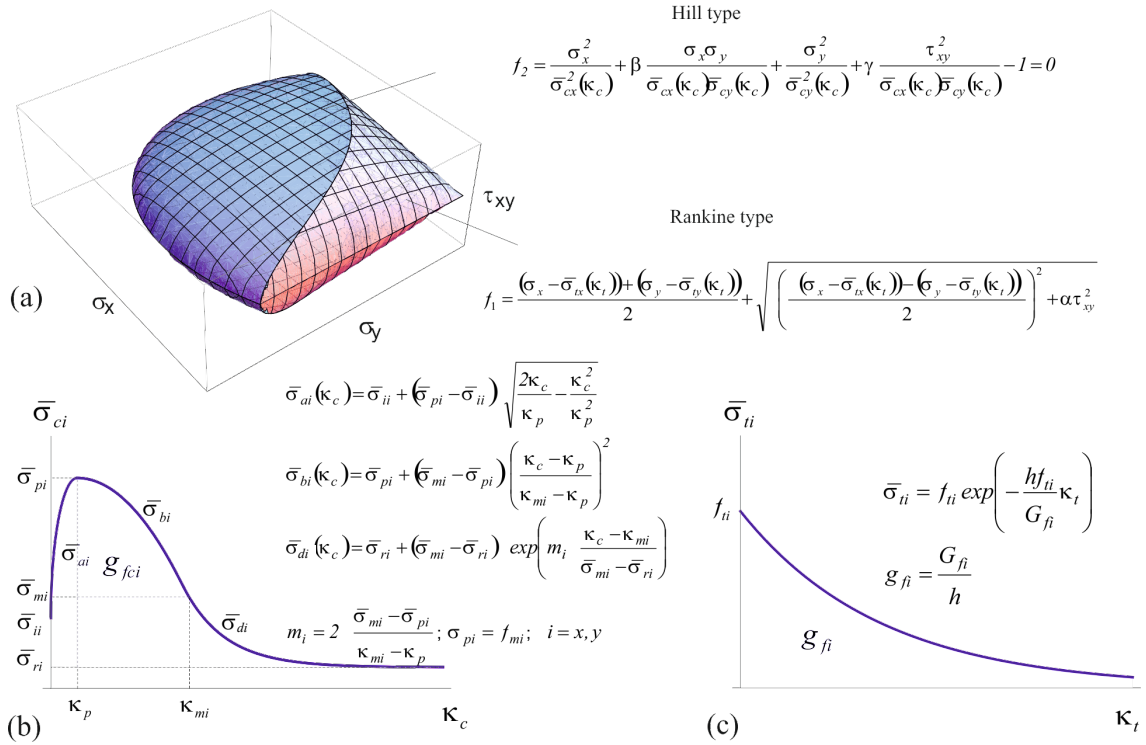


Figure 12. (a) Biaxial strength envelope for masonry; stress-strain laws adopted for the material in (b) uniaxial compression and (c) uniaxial tension [32-34].

If these experimental tests are performed under displacement control, they also provide the five required inelastic parameters, that is to say fracture energies in tension G_{fi} and compression G_{fci} in both directions x - y , as well as the plastic strain corresponding to the peak compressive strength, κ_p . The complete calibration of the model also requires additional non-standard tests [34] in order to determine the three remaining parameters α , β and γ (Figure 12a); in more detail, α weights the shear stress contribution to tensile failure, β controls the coupling between normal stress values in

case of compressive failure and γ weights the shear stress contribution to compressive failure.

3.2 Calibration of the model for AAC masonry

3.2.1 Biaxial failure envelope

The parameters required for the construction of the failure envelope proposed by Lourenço et al. have been derived on the basis of the results provided by the previously described experimental tests on AAC masonry elements. The compressive strengths in the two main directions x, y - respectively obtained as the average peak stress values σ_v for PMC90 and PMC0 samples (see Table 1) - have been assumed equal to $f_{mx} = f_{my} = 2.60$ MPa. The direct tensile strengths, respectively equal to $f_{tx} = 0.29$ MPa and $f_{ty} = 0.24$ MPa, have been instead determined numerically, by simulating the three-point bending tests carried out on samples BMF0 and BMF90 (Table 4), as better described in Section 3.2.2.

The parameter α has been calculated through the least squares method, by minimizing the function $\sum f_{1,j}^2(\alpha)$ with the non-linear optimization algorithm of Levenberg-Marquard, being $f_{1,j}$ the plastic potential in the j -th experimental point (Figure 12a); in this way, the value of $\alpha = 0.5$ has been obtained. Similarly, the parameters β and γ have been calculated by minimizing the function $\sum f_{2,j}^2(\beta, \gamma)$, so obtaining $\beta = -0.6$ and $\gamma = 5$.

The so calibrated failure envelope is depicted in Figure 13 in the $\sigma_x - \sigma_y$ plane, through level curves corresponding to different values of the applied shear stress τ_{xy} , respectively equal to 0, 0.76, and 1.09 MPa. On the same graph, the corresponding

experimental values obtained from uniaxial and biaxial compression tests (Section 2.2), as well as from three-point bending (Section 2.3) and diagonal compression ones (Section 2.4), are also reported; as can be seen, the model error appears to be comparable with the experimental scattering. Furthermore, the obtained curves show that the behavior of AAC masonry is characterized by a weak anisotropy, with similar strength values in the two main directions x, y .

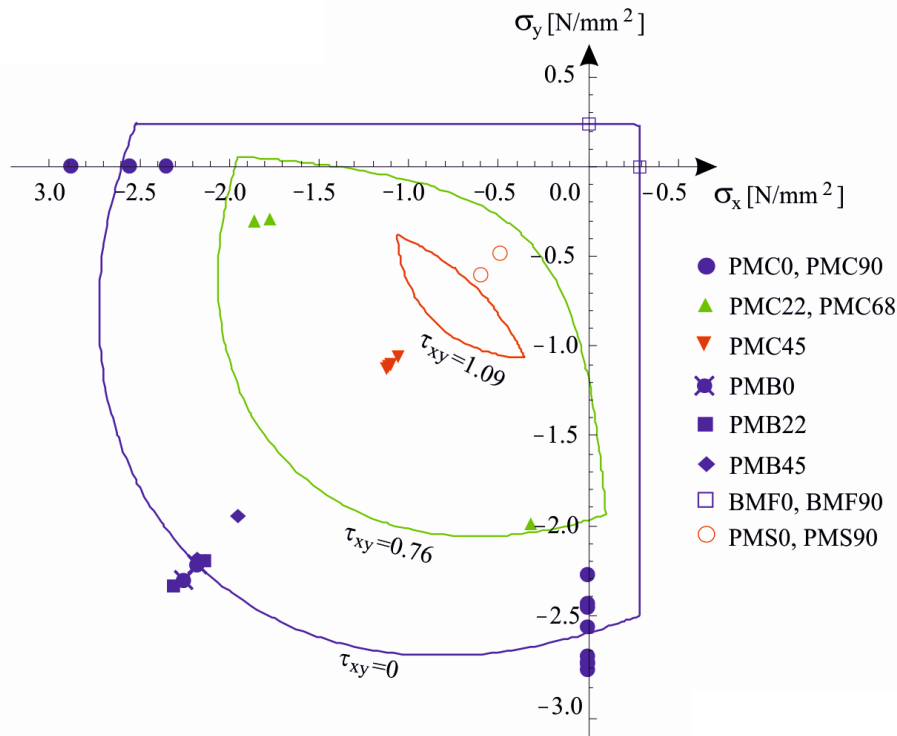


Figure 13. Comparison between the adopted failure envelope [32-34] and the experimental results obtained for AAC masonry for different values of the applied shear stress τ_{xy} .

3.2.2 Stress-strain laws in uniaxial compression and tension

Based on the experimental results, the plastic stress-strain laws for uniaxial compression in the two main directions – whose equations are reported for reading convenience in Figure 12b – have been calibrated by adopting the average values of compressive strengths ($f_{mx} = f_{my} = 2.60$ MPa), and elastic moduli ($E_x = 1700$ MPa,

$E_y = 1400 \text{ MPa}$). The plastic strain corresponding to the peak compressive strength has been assumed equal to $\kappa_p = 0.3\%$. The two fracture energies in compression have been deduced numerically, through an inverse procedure based on the fitting of all the available experimental data (Figure 14 a-b), so as to take into account the important scatter of the softening branches. Since the experimental response was quite similar in the two main directions (Figure 14c), also in this case a unique value of $g_{fcx} = g_{fcy} = 2.26 \cdot 10^{-3} \text{ N/mm}^2$ has been adopted. This value corresponds only to the local contribution of the $\bar{\sigma}_{ci} - \kappa_c$ diagram (where the subscript i refers to the material axis) and therefore the basis for its definition is only numerical, in order to obtain objective results with respect to mesh refinement [32].

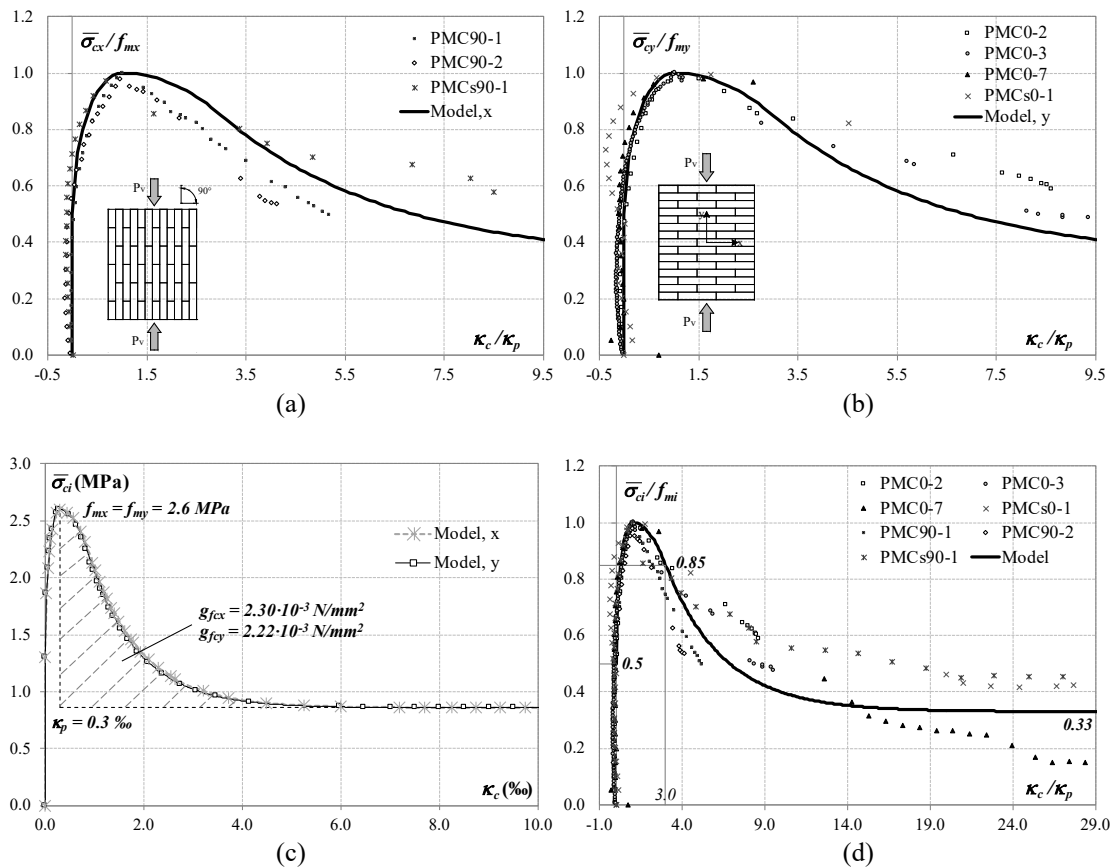


Figure 14. Comparisons between the adopted inelastic law in compression for AAC masonry and the available experimental data in (a) x and (b) y directions; (c) main parameters of the adopted laws in x

and y; (d) definition of a unique inelastic law and comparison with all the experimental results.

The complete inelastic law adopted for compression in both the considered directions, respectively parallel and perpendicular to bed joints, is reported in Figure 14d in the dimensionless plane $\bar{\sigma}_{ci} / f_{mi} - \kappa_c / \kappa_p$, where it is compared with the available experimental data (specimens PMC0, PMCs0, PMC90, and PMCs90). On the same Figure, the new parameters used herein for the definition of the shape of the curve are also reported, that is to say $\bar{\sigma}_{ii} / f_{mi} = 0.5$, $\bar{\sigma}_{mi} / f_{mi} = 0.85$, $\bar{\sigma}_{ri} / f_{mi} = 0.33$, with reference to the nomenclature adopted in Figure 12b and according to [32]. Moreover, with the previous assumptions, parameter κ_{mi} becomes:

$$\kappa_{mi} = \frac{1080}{1627} \frac{G_{fci}}{h f_{mi}} + \kappa_p. \quad (3)$$

The stress-strain laws in uniaxial tension – whose equations are reported in Figure 12c – have been instead calibrated by hypothesizing the same elastic moduli obtained for compression and by adopting the average fracture energies determined from three-point bending tests on BMF0 and BMF90 samples (respectively equal to $G_{fx} = 7.10 \cdot 10^{-3}$ N/mm and $G_{fy} = 5.15 \cdot 10^{-3}$ N/mm, see Table 4). Direct tensile strengths have been obtained from inverse analysis by using the general-purpose FE code ABAQUS to simulate the above-mentioned three-point bending tests. To this scope, each beam has been modeled by adopting a regular mesh formed by square 4-nodes plane stress elements (CPS4 in the adopted FE code library), with 5 mm side, and this discretization has been further refined in correspondence of the supports and of the loading plate (Figure 15d). The problem of mesh dependence has been overcome by scaling the fracture energies through the equivalent length $h = \sqrt{A_e}$, where A_e is the

area of the adopted element [33].

The interaction between the supports and the masonry sample has been taken into account by introducing contact elements and by considering friction between AAC and steel. The analyses have been performed by adopting quasi-static loading control to overcome convergence problems, so obtaining the complete load-deflection curve. The computed tensile strength average values in the two main masonry directions are respectively equal to $f_{tx} = 0.29$ MPa and $f_{ty} = 0.24$ MPa.

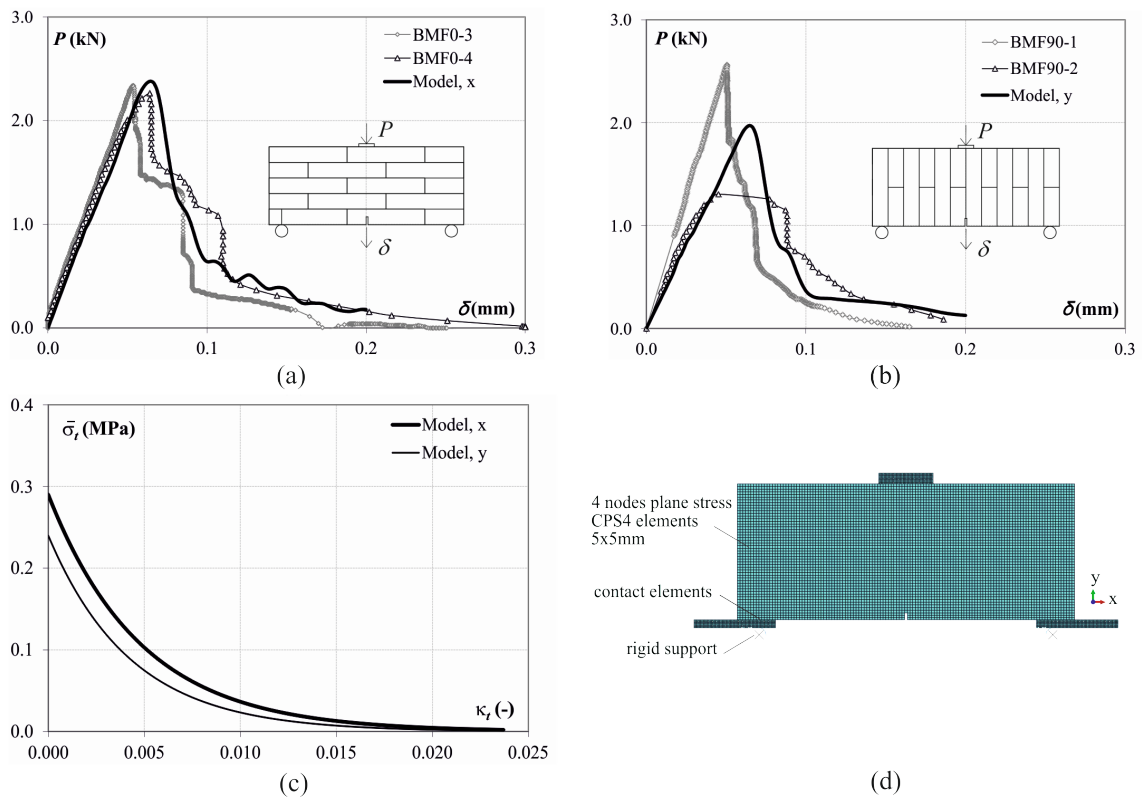


Figure 15. Comparisons between numerical and experimental curves obtained for AAC masonry beams (BMF) in terms of applied load P vs. midspan deflection δ in (a) x and (b) y directions. (c) Adopted inelastic law in tension for AAC masonry in x and y directions; (d) FE mesh of AAC masonry beams.

Figure 15a-b shows the comparison between numerical and experimental results in terms of applied load P vs. midspan deflection δ , in case of BMF0 (Figure 15a) and BMF90 samples (Figure 15b). As can be observed, in the first case (x direction)

experimental results are almost superimposed with each other and with the numerical curve. On the contrary, experimental results relative to y direction present a larger scatter, which is due to the different characteristics of the examined samples. As already mentioned, specimen BF90-1 was indeed formed by an odd number of units, with the notch placed at half-width of the central brick line, while specimen BMF90-2 was realized with an even number of units, with the notch placed exactly in correspondence of the glue joint. As regards numerical modeling, the geometry of specimen BMF90-2 has been considered, while the adopted mechanical properties have been set equal to the average values deduced from tests, so obtaining an intermediate response.

Finally, Figure 15c reports the corresponding exponential softening plastic stress-strain relations $\bar{\sigma}_{ti}-\kappa_t$ in x and y directions.

4. SIMULATION OF THE BEHAVIOR OF A FULL-SCALE AAC MASONRY WALL

The effectiveness of the so calibrated plastic model and its ability of correctly describe the behavior of AAC masonry structures has been subsequently verified through the simulation of an experimental test carried out at the University of Pavia on a full-scale AAC masonry wall subjected to a vertical load and an increasing in-plane horizontal force [31]. The geometry and the adopted test arrangement are schematized in Figure 16a. As can be seen, the considered wall was 1.5 m long, 2.75 m high and 0.3 m wide, and it was assembled by using $625 \times 300 \times 250$ mm AAC blocks, which are bigger than those used to calibrate the adopted constitutive model. The specimen was built with thin mortar layers (2-3 mm thick) and filled head joints. Reinforced concrete

beams – whose dimensions can be found in [31] – were built at the top of the wall, to guarantee a better load distribution, and at the bottom, acting as a foundation. The chosen test setup was indeed a cantilever system (fixed at the base and free at the top) with a constant vertical load of 200 kN applied on the top beam through hydraulic jacks. The horizontal load was instead applied through a displacement-controlled horizontal hydraulic actuator, performing three fully reversed cycles for the chosen target displacement level, until the reaching of a horizontal displacement equal to 0.6% of the wall height [31].

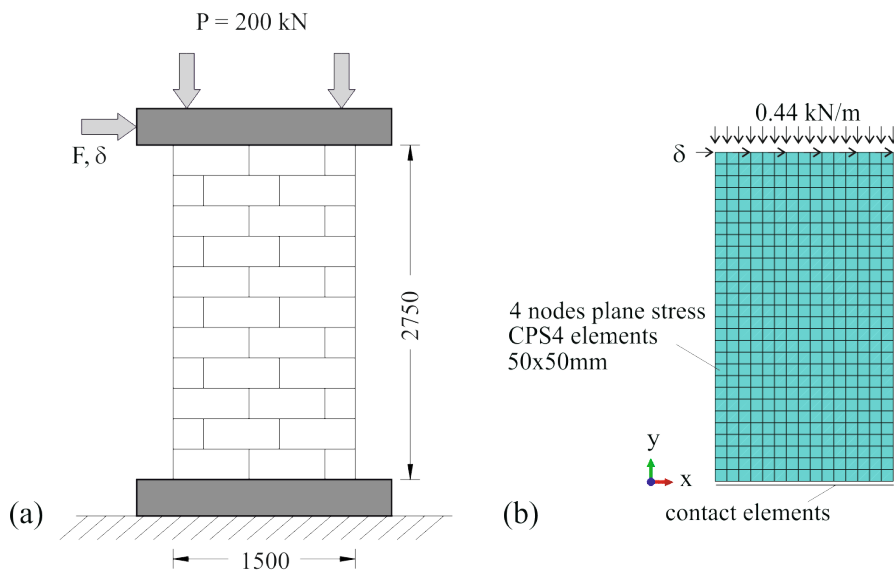


Figure 16. Tests on a full scale AAC masonry wall: (a) sketch of the experimental setup [31]; (b) adopted FE mesh.

The considered wall has been modeled by adopting a uniform mesh, formed by square 4-node plane stress elements (CPS4) with 50 mm side, as shown in Figure 16b. For sake of simplicity, the two reinforced concrete beams have not been included in the FE model, by simply introducing contact elements at the base and considering friction between the AAC wall and the support. The horizontal force has been replaced by a uniform distribution of prescribed displacements δ . The mechanical behavior of AAC

masonry has been simulated through the constitutive model described in the previous Section. Since the mechanical properties of AAC blocks used for the realization of the examined wall were not exactly the same of those determined in the experimental program illustrated herein, both the compressive strengths as well as the elastic moduli were properly updated, according to the corresponding values reported in [31]. In more detail, the following values have been assumed: $f_{mx} = 1.90$ MPa, $f_{my} = 2.20$ MPa, $E_x = E_y = 1498$ MPa. On the contrary, for the other required elastic and inelastic properties – which were not available in [31] - the values determined in Section 3 have been assumed. This modeling choice seems to be reasonable, since the adopted model is based on an orthotropic formulation and also its calibration to the case of AAC masonry is based on weakly anisotropic data (e.g. the elastic moduli in the two principal directions are different). As a consequence, the adoption of slightly different strength values in the two principal direction (which are anyway comparable with those adopted in Section 3), should not alter the effectiveness of the proposed approach.

The NLFE analysis has been carried out under displacement control, by simply modeling the last loading cycle. Also in this case, a quasi-static analysis has been performed to mitigate convergence problems, and the controlled displacement has been increased monotonically up to failure. The so obtained results have been reported in terms of applied load F vs. top horizontal displacement δ in Figure 17, where they are compared with the experimental response. The latter represents the envelope curve of the three fully reversed cycles performed during the test. As can be observed, the model is able to describe with sufficient accuracy the behavior of the examined full-scale wall until the reaching of the ultimate load, whose value is also predicted.

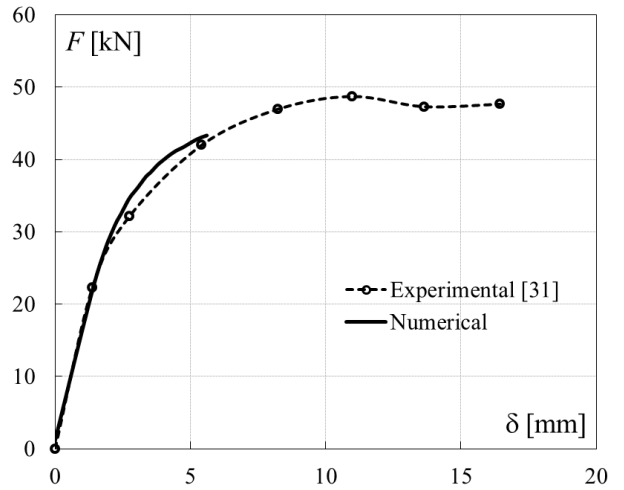


Figure 17. Comparison between numerical and experimental results in terms of applied load F vs. horizontal displacement δ .

Anyhow, it should be underlined that the numerical response appears to be significantly less ductile than the experimental one. The underestimated ductility is due to important convergence problems that have been reported also in other works that adopt the same algorithm [43, 44]. In particular, van der Meer [44] analyzed the reasons of the convergence weakness of the subroutine (apex, return-mapping, multi-surface plasticity algorithm) and proposed some promising improvements that are, however, out of the scope of this work.

5. CONCLUSIONS

The present work illustrates the main results of an experimental program focused on the mechanical characterization of AAC masonry. To this aim, the following test typologies have been performed:

- uniaxial compression tests on masonry panels under force/displacement control;
- biaxial compression tests on masonry panels;

– diagonal compression tests on small masonry panels;
– three-point bending tests on masonry beams under force/CMOD control.
The results have been used to calibrate a well-known macroscopic anisotropic constitutive model already developed for ordinary masonry and available in the technical literature [32-34]. This model has been subsequently applied to simulate numerically the behavior of a full-scale AAC masonry wall subjected to a pushover test [31].

The main conclusions of this research are summarized herein:

- if properly calibrated, numerical anisotropic models proposed for traditional masonry can be also used for AAC masonry;
- AAC masonry is characterized by a very weak anisotropy due to the particular cementitious glue adopted for the realization of thin joints;
- observed failure modes reveal that if joints are correctly realized by skilled labor, they do not represent a significant weakness in masonry behavior.

For these reasons, as a first approximation, the mechanical properties of the raw AAC material (with a similar density and moisture content) can be used for mechanical models and finite element simulations on masonry elements.

ACKNOWLEDGEMENTS

Mr. Matteo Riva is gratefully acknowledged for his contribution in the execution of experimental tests. The authors would also like sincerely to thank Prof. Ivo Iori and M.Sc. Eng. Giuseppe Gazzola for their interest and scientific support in this research.

REFERENCES

- [1] Narayanan N, Ramamurthy K. Structure and properties of aerated concrete: a review. *Cem Concr Compos* 2000; 22: 321-329.
- [2] Laukaitis A, Fiks B. Acoustical properties of aerated autoclaved concrete. *Appl Acoust* 2006; 67: 284-296.
- [3] Limbachiya MC, Roberts JJ Eds. *Proc. 4th Int Conf on AAC - Autoclaved Aerated Concrete: innovation and development*. Taylor & Francis, London, 2005.
- [4] Wittmann FH Eds. *Proc. 3rd RILEM Int Symp on AAC - Advances in Autoclaved Aerated Concrete*. Balkema, Rotterdam, 1992.
- [5] Aroni S, De Groot GJ, Robinson MJ, Svanholm G, Wittmann FH Eds. *Autoclaved aerated concrete: properties, testing and design*. RILEM Recommended Practice, London: E&FN Spon, 1993.
- [6] Marzahn GA. Extended investigation of mechanical properties of masonry units. *LACER* 2002; 7: 237-254.
- [7] Muszynski LC, Gulas S. Fire resistance and performance of alternative concrete wall systems. *J Constr Edu* 2001; 6: 146-154.
- [8] Delmotte P, Rivillon P, Wesierski V, Hurez M. Study on shear walls realized with autoclaved aerated concrete masonry (in French). *Cahier du CSTB n. 3492, Livraison* 445, 2003.
- [9] Klingner RE, Tanner JE, Varela JL, Barnett RE. Autoclaved aerated concrete: innovative materials and civil infrastructure. *Proc. Int Work on Innovation in Materials and Design of Civil Infrastructure*, Cairo, 2005: 1-36.
- [10] Tanner JE, Varela JL, Klingner RE, Brightman MJ, Cancino U. Seismic testing of autoclaved aerated concrete shearwalls: a comprehensive review. *ACI Struct J* 2005;

734 102(3): 374-382.

735 [11] Wittmann FH Eds. Autoclaved Aerated Concrete, Moisture and Properties. Elsevier,
736 Amsterdam, 1983.

737 [12] Lourenço PB. Experimental and numerical issues in the modelling of the mechanical
738 behavior of masonry. In Roca P et al Eds: Structural Analysis of Historical
739 Constructions II. Barcelona: CIMNE, 1998, pp. 57-91.

740 [13] Johnson FB, Thompson JN. Development of diametric testing procedures to provide
741 a measure of strength characteristics of masonry assemblages. In Johnson FH Ed:
742 Designing, Engineering and Constructing with Masonry Products, Gulf Publishing,
743 Houston, 1969, pp. 51-57.

744 [14] Drysdale RG, Hamid AA. Behavior of concrete block masonry under axial
745 compression. Amer Concr Inst J 1979; 76(6): 707-721.

746 [15] Hamid AA, Drysdale RG. Proposed failure criteria for concrete block masonry under
747 biaxial stresses. ASCE J Struct Div 1981; 107(8): 1675-1687.

748 [16] Samarasinghe W, Hendry AW. The strength of brickwork under biaxial tension-
749 compression. In: Proc 7th Int Symp on Load Bearing Brickwork, London, 1980, pp.
750 129-140.

751 [17] Page AW. The biaxial compressive strength of brick masonry. Proc Instn Civ Engrs
752 1981; 71(2): 893-906.

753 [18] Page AW. The strength of brick masonry under biaxial compression-tension. Int J
754 Masonry Constr 1983; 3(1): 26-31.

755 [19] Dhanasekar M, Page AW, Kleeman PW. The failure of brick masonry under biaxial
756 stresses. Proc Instn Civ Engrs 1985; 79(2): 295-313.

757 [20] Dhanasekar M, Kleeman PW, Page AW. Biaxial stress-strain relations for brick

758 masonry. ASCE J Struct Eng 1985; 111(5): 1085-1100.

759 [21] Hegemier GA, Nunn RO, Arya SK. Behavior of concrete masonry under biaxial
760 stresses. Proc North Amer Masonry Conf, Univeristy of Colorado, Boulder, 1978, pp.
761 1.1-1.28.

762 [22] Mojsilović N. Strength of masonry subjected to in-plane loading: A contribution. Int
763 J Solid Struct 2011; 48: 865-873.

764 [23] Badarloo B, Tasnimi AA, Mohammadi MS. Failure criteria of unreinforced grouted
765 brick masonry based on a biaxial compression test. Scientia Iranica Civ Eng 2009;
766 16(6): 502-511.

767 [24] da Porto F. In Plane Cyclic Behaviour of Thin Layer Joint Masonry. PhD Thesis,
768 University of Trento, Italy, 2005.

769 [25] Dhanasekar M, da Porto F. Review of the progress in thin bed technology for
770 masonry construction. In: 11th Canadian Masonry Symposium, Toronto, Ontario,
771 2009, pp. 1003-1014.

772 [26] Fried AN, Marrocchino E, Bradsell C, Roberts JJ. Unreinforced Solid Dense
773 Concrete Block Walls Constructed Using Thin Bed Technology, Structural Engineer
774 UK, 2005, 83(12): 33-37.

775 [27] Thamboo J A, Dhanasekar M, Yan C. Characterisation of flexural bond strength in
776 thin bed concrete masonry. In: 15th Int Brick and Block Masonry Conf. Federal
777 University of Sao Carlos and Federal University of Santa Catarina, 2012.

778 [28] Vermeltfoort A. Shear, Bond and 2D Compressive Properties of Thin Bed Mortar
779 Masonry. In: Proc. 13th Int Brick and Block Masonry Conf, Amsterdam, 2004, pp. 1-
780 10.

781 [29] Tanner JE, Varela JL, Klingner RE, Fouad FH, Barnett RE. Technical basis for US

782 design provisions for Autoclaved Aerated Concrete masonry. In Limbachiya et al. Eds:
783 Autoclaved Aerated Concrete, Innovation and Development, Taylor & Francis,
784 London, 2005, pp. 325-336.

785 [30] Shermer D. Seismic behavior of Autoclaved Aerated Concrete masonry
786 constructions. In Limbachiya et al. Eds: Autoclaved Aerated Concrete, Innovation and
787 Development, Taylor & Francis, London, 2005, pp. 387-394.

788 [31] Costa AA, Penna A, Magenes G. Seismic Performance of Autoclaved Aerated
789 Concrete (AAC) Masonry: From Experimental Testing of the In-Plane Capacity of
790 Walls to Building Response Simulation. J Earthquake Eng 2011; 15(1): 1-31.

791 [32] Lourenço PB. Computational strategies for masonry structures. Ph.D. Thesis, TU
792 Delft, The Netherlands, 1996.

793 [33] Lourenço PB, De Borst R, Rots JG. A plane stress softening plasticity model for
794 orthotropic materials. Int J Numer Meth Eng 1997; 40: 4033-4057.

795 [34] Lourenço PB, Rots JG, Blaauwendraad A. Continuum model for masonry parameter
796 estimation and validation. ASCE J Struct Eng 1998; 124(6): 642-652.

797 [35] Ferretti D, Michelini E, Rosati G. Cracking in autoclaved aerated concrete:
798 Experimental investigation and XFEM modeling. Cem Concr Res 2015; 67: 156-167.
799 doi: 10.1016/j.cemconres.2014.09.005.

800 [36] Ferretti D, Gazzola G, Iori I, Michelini E, Rosati G. Calibration of a nonlinear
801 anisotropic mechanical model for AAC masonry (in Italian). Proc. 18th C.T.E.
802 Congress, Brescia, 2010, pp.153-162.

803 [37] Wittmann FH, Gheorghita I. Fracture toughness of autoclaved aerated concrete. Cem
804 Concr Res 1984; 14: 369-374.

805 [38] Trunk B, Schober G, Helbling AK, Wittmann FH. Fracture mechanics parameters of

806 autoclaved aerated concrete. Cem Concr Res 1999; 29: 855-859.

807 [39] UNI EN 1996-1-1:2006. Eurocode 6 - Design of masonry structures - Part 1-1:

808 General rules for reinforced and unreinforced masonry structures.

809 [40] Tanner JE. Design provisions for autoclaved aerated concrete (AAC) structural

810 systems. PhD Thesis, University of Texas, Austin, 2003.

811 [41] Lourenço PB, Palácio K, Prieto F. Implementation of a constitutive model for

812 masonry shells as a stand-alone subroutine. Report 02-DEC/E-13, Universidade do

813 Minho, Departamento de Engenharia Civil, 2002.

814 [42] ABAQUS 6.12. Online Documentation. Dassault Systèmes Simulia Corp.

815 [43] Dhanasekar M, Haider W. Explicit finite element analysis of lightly reinforced

816 masonry shear walls. Comp & Struct 2008; 86(1), 15-26.

817 [44] van der Meer LJ, Unbonded post-tensioned shear walls of calcium silicate element

818 masonry, PhD Thesis, Eindhoven University of Technology, 2013, ISBN: 978-90-386-

819 3374-9.

820

LIST OF FIGURES

Figure 1. General view of some of the AAC masonry specimens tested during the experimental program.

Figure 2. Sketch of uniaxial compression tests on masonry panels (a) PMC and (b) PMCs (characterized by reduced dimensions).

Figure 3. General setup of uniaxial compression tests performed under loading control: (a) not instrumented and (b) instrumented small-scale masonry panels (PMC).

Figure 4. General setup of uniaxial compression tests performed under displacement control: (a) small-scale masonry panels (PMC) and (b) square specimens with reduced dimensions (PMCs).

Figure 5. Uniaxial compression tests on homogeneous AAC samples: (a) cubes with an edge length of 40 mm and (b) panels with the same geometry and dimensions of PMC masonry ones.

Figure 6. Uniaxial compression tests on AAC masonry panels (PMC): observed crack patterns at failure as function of bed joint inclination.

Figure 7. (a) Sketch of biaxial compression tests on masonry panels (PMB); (b) sketch and (c) general view of the adopted setup.

Figure 8. Biaxial compression tests on AAC masonry panels (PMB): observed crack patterns at failure as function of bed joint inclination.

Figure 9. Three-point bending tests on AAC masonry beams BMF (a) without and (b) with notch: adopted setup.

Figure 10. Sketch of three-point bending tests on AAC masonry beams BMF: (a) unnotched specimens BMF0; specimens (b) BMF0 and (c) BMF90 with a central notch.

Figure 11. (a) Sketch and (b) adopted arrangement of diagonal compression tests on small AAC masonry panels PMS; (c) observed failure mode.

Figure 12. (a) Biaxial strength envelope for masonry; stress-strain laws adopted for the material in (b) uniaxial compression and (c) uniaxial tension [32-34].

Figure 13. Comparison between the adopted failure envelope [32-34] and the experimental results

obtained for AAC masonry for different values of the applied shear stress τ_{xy} .

Figure 14. Comparisons between the adopted inelastic law in compression for AAC masonry and the available experimental data in (a) x and (b) y directions; (c) main parameters of the adopted laws in x and y; (d) definition of a unique inelastic law and comparison with all the experimental results.

Figure 15. Comparisons between numerical and experimental curves obtained for AAC masonry beams (BMF) in terms of applied load P vs. midspan deflection δ in (a) x and (b) y directions. (c) Adopted inelastic law in tension for AAC masonry in x and y directions; (d) FE mesh of AAC masonry beams.

Figure 16. Tests on a full scale AAC masonry wall: (a) sketch of the experimental setup [31]; (b) adopted FE mesh.

Figure 17. Comparison between numerical and experimental results in terms of applied load F vs. horizontal displacement δ .

LIST OF TABLES

Table 1. Uniaxial compression tests on AAC masonry panels (PMC and PMCs): effective dimensions of the specimens and experimental failure loads.

Table 2. Uniaxial compression tests on AAC masonry panels (PMC and PMCs): elastic moduli E_x , E_y , Poisson ratio ν and compressive peak strains ϵ_{px} and ϵ_{py} .

Table 3. Biaxial compression tests on AAC masonry panels (PMB): effective dimensions of the specimens and experimental failure loads.

Table 4. Three-point bending tests on AAC masonry beams (BMF): effective dimensions of the specimens, experimental failure loads, indirect tensile strengths and fracture energies in tension.

Table 5. Diagonal compression tests on small AAC masonry panels (PMS): effective dimensions of the specimens and experimental failure loads.